Int. J. Electrochem. Sci., 16 **(2021)** Article ID: 210312, doi: 10.20964/2021.03.57

International Journal of
ELECTROCHEMICAL
SCIENCE
www.electrochemsci.org

Use of Lignin-Derived Carbon to Prepare Nickel-Based Electrocatalysts for Water Splitting

Jia Hui[1], *Meng Xiang*[2], *Jianxiang Chen*[2], *Shilong Zhou*[2], *Yin Cheng*[1,*] *and Zhou Yang*[2,*]

[1] Engineering Technology and Materials Research Center, China Academy of Transportation Sciences, Beijing 100029, China
[2] Department of Material Engineering, Jiangsu University of Technology, Changzhou 213001, China
[*]E-mail: by0913108@buaa.edu.cn, zhouyang@jsut.edu.cn

Received: 18 November 2020 / *Accepted:* 8 January 2021 / *Published:* 31 January 2021

Water splitting is the most feasible way of obtaining hydrogen energy, but the high overpotential of the electrocatalytic materials conventionally used for water splitting create a bottleneck in the process. Herein, we prepare a NiS_x/C-780 electrocatalyst derived from lignin and nickel that exhibits good electrocatalytic properties and for which the overpotential of 358 mV at 10 mA cm^{-2} for the oxygen evolution reaction (OER) and the Tafel slope of 107.7 mV dec^{-1} are superior to those of commercial RuO_2. This study serves as a reference for designing low-cost and environmentally friendly electrocatalysts for water splitting.

Keywords: lignin, water splitting, nickel, electrocatalyst

1. INTRODUCTION

The energy crisis has become a severe problem worldwide that has motivated the search for new forms of energy. Among the numerous forms of energy available, hydrogen is outstanding in being nonpolluting and having a high heat value [1]. Hydrogen can be obtained by water splitting [2]. However, the excessively high overpotentials of the hydrogen evolution reaction (HER) and the oxygen evolution reaction (OER) raise the cost of water splitting [3]. The high cost of traditional electrocatalyst materials, which are mainly precious metal oxides, such as RuO_2 and IrO_2, has created a demand for substitutes [4-6].

Carbon materials have a low cost and high conductivity and have therefore been investigated for energy storage and catalysis applications over recent years [7-9]. Carbon sources are quite widespread, and biomass produced in daily life can be used as a carbon precursor [10-12]. However, the few active sites in carbon materials typically negatively affect electrocatalytic properties [13,14]. Therefore, we introduced heteroatoms to activate carbon materials [15,16]. He et al. [17] synthesized 3D Co-Bi/BNC

by doping a litchi pericarp with Co and B, resulting in excellent OER performance, corresponding to an OER overpotential as low as 286 mV at 10 mA cm^{-2} and a small Tafel slope.

Lignin is a renewable biopolymer that is typically separated from lignocellulosic biowaste in a destructive manner [18,19]. Carbon is the main element in the heterogeneous structure of lignin, which is therefore a good candidate carbon source [20,21]. We used lignin as a carbon source and $Ni(NO_3)_2$ as a nickel source in this study to synthesize carbon nanocomposites, where the heteroatoms in lignin (including S and O) combine with Ni to form metal nanocompounds that activate carbon [22]. The as-obtained product NiS_x/C-780 exhibits good electrocatalytic performance, with an OER overpotential of 358 mV at 10 mA cm^{-2} and a Tafel slope of 107.7 mV dec^{-1}.

2. EXPERIMENTAL

2.1 Materials

Lignin was purchased from Aladdin Chemical Company. RuO_2, Pt/C (20%) and 5% Nafion perfluorinated resin were purchased from Macklin Chemical Company. $Ni(NO_3)_2 \cdot 6H_2O$ and ethanol were purchased from Shanghai Lingfeng Chemical Company.

2.2 Preparation

Lignin was dried at 80°C for 12 h, followed by dispersing 4 g of lignin and 0.365 g of $Ni(NO_3)_2 \cdot 6H_2O$ in 35 mL of deionized water under 0.5 h of stirring. The solution mixture was transferred to a hydrothermal reactor, which was maintained at 120°C for 10 h. The as-reacted product was collected, dried and mixed with K_2CO_3 in a 1:3 weight ratio, followed by calcination in a tube furnace at 600, 700 and 780°C for 2 h under nitrogen (100 mL min^{-1}). Finally, the product was thoroughly washed with deionized water and ethanol and dried at 60°C. The as-obtained product was labeled NiSx/C-y (where y represents the calcination temperature).

2.3 Characterization

The material microstructure was observed by field-emission scanning electron microscopy (FE-SEM, Sigma 500) and transmission electron microscopy (TEM, JEM-2100). The chemical properties were characterized by X-ray diffraction (XRD), X-ray photoelectron spectroscopy (XPS, PHI 5000CESCA), and Raman spectroscopy (XploRA). The electrocatalytic performance of the glass carbon electrode coating on the samples was tested using linear sweep voltammetry (LSV), cyclic voltammetry (CV) and electrochemical impedance spectroscopy (EIS) with an electrochemical workstation (Chenhua, CHI 760E). Graphite and Hg/HgO electrodes were used as the counter and reference electrodes, respectively, in a 1 M KOH electrolyte.

3. RESULTS AND DISCUSSION

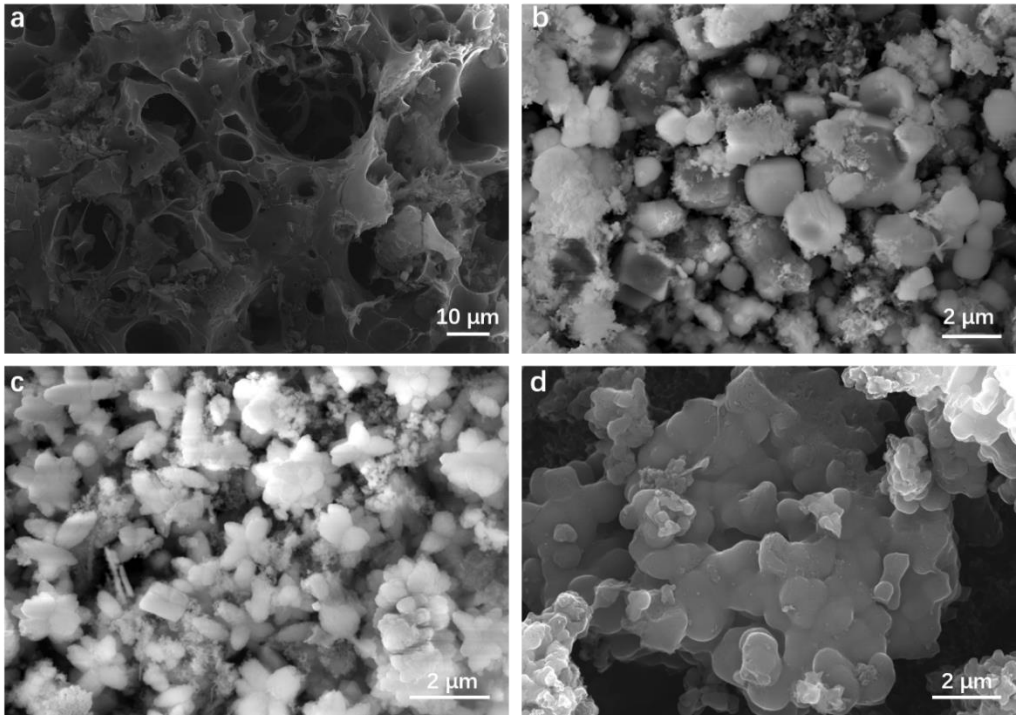

Figure 1. FESEM images of (a) lignin; (b) NiS_x/C-600; (c) NiS_x/C-700; and (d) NiS_x/C-780

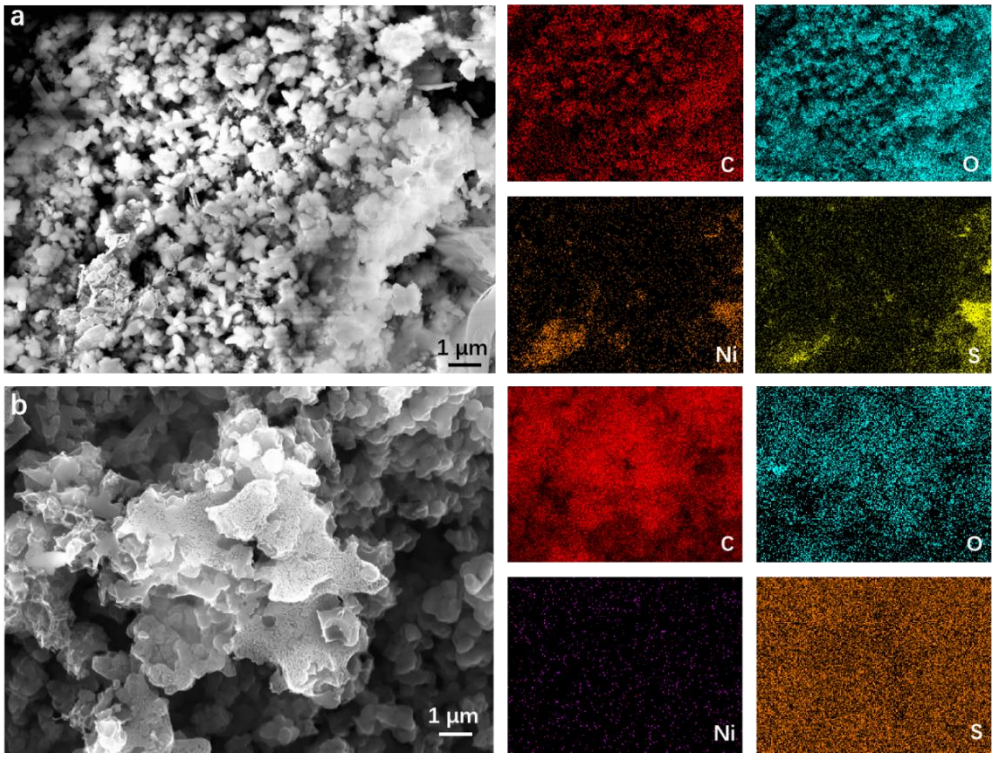

Figure 2. Element mapping images of (a) NiS_x/C-700 and (b) NiS_x/C-780

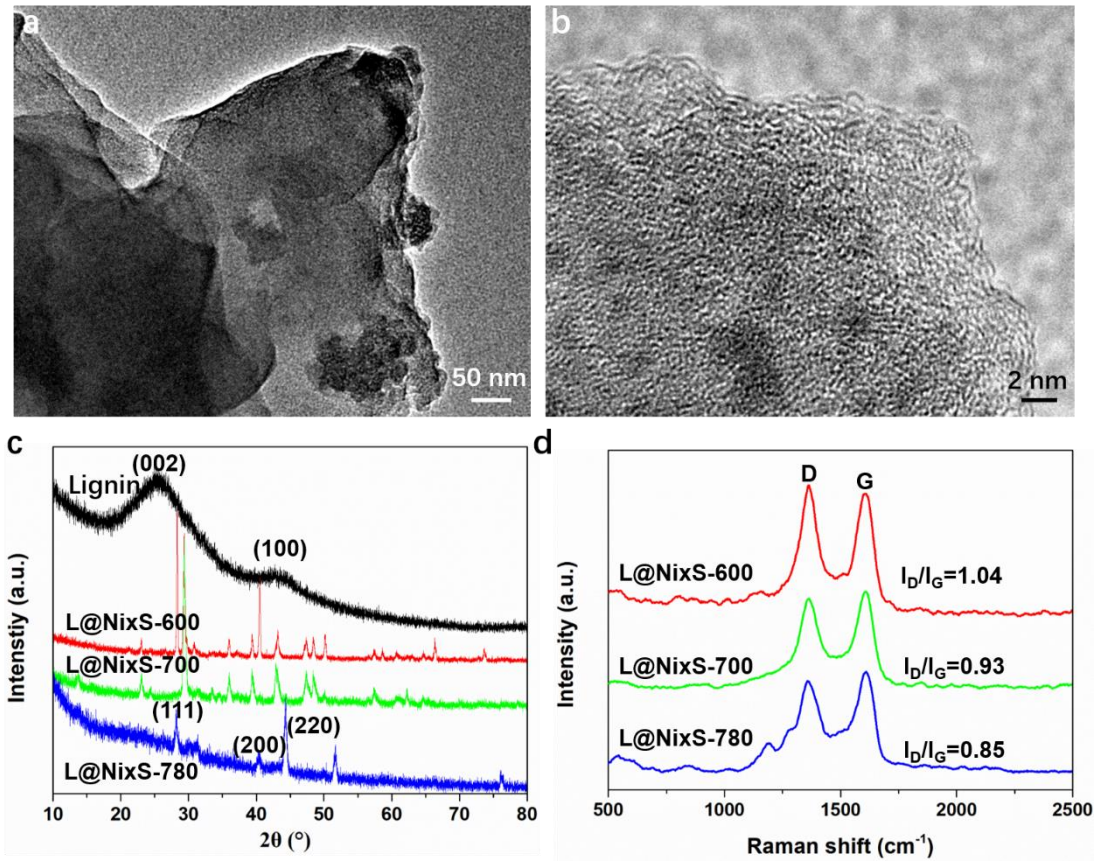

Figure 3. (a) TEM image and (b) HR-TEM image of NiS_x/C-780; (c) XRD patterns of lignin, NiS_x/C-600, NiS_x/C-700 and NiS_x/C-780; and (d) Raman spectra of NiS_x/C-600, NiS_x/C-700 and NiS_x/C-780

Fig. 1 shows FE-SEM images of all the samples. Fig. 1a shows a typical bulk carbon structure for lignin. Fig. 1b, 1c and 1d show the growth of polygon nanoparticles on carbon after high-temperature calcination. Among the investigated samples, NiS_x/C-600 exhibits a cubic structure, whereas NiS_x/C-700 exhibits a star structure. However, abnormal lamella-like nanoparticles appear in NiS_x/C-780. Figs. 2a and 2b shows the results of element mapping of NiS_x/C-700 and NiS_x/C-780 used to analyze the constituent species. The star-like species in NiS_x/C-700 are carbon compounds, with clear growth of Ni_xS on carbon. However, NiS_x/C-780 is mainly occupied by C and O and has a very low Ni content. As NiS has a melting point of 797°C, most of the NiS melted under calcination at 780°C. Figs. 3a and 3b shows TEM images of NiS_x/C-780, in which a lamellar structure attached to a small quantity of nanoparticles can be seen in Fig. 3a, and typical crystal stripes of graphite carbon can be observed in Fig. 3b.

We further confirmed the main component of NiS_x/C-y by analyzing the XRD patterns of lignin and NiS_x/C-y, as shown in Fig. 3c. Lignin exhibits two typical carbon peaks at 26° and 43°, which correspond to (002) and (100). NiS_x/C-600 and NiS_x/C-700 exhibit complex peaks, which can be ascribed to NiS and Ni_3S_4 [23-25] and were thus labeled Ni_xS. The few weak peaks for NiS_x/C-780 indicate a low Ni_xS content. It is noteworthy that the sharp peaks of the Ni_xS crystal may cover the carbon lattices in NiS_x/C-600 and NiS_x/C-700, whereas the indistinct carbon peaks in NiS_x/C-780 result

from the low Ni_xS content.

The Raman spectra presented in Fig. 3d exhibit two distinct characteristic peaks at approximately 1360 cm^{-1} and 1590 cm^{-1}, which are attributed to the disordered sp^3 (D band) and graphitic sp^2 (G band) of carbon, respectively [26]. The intensity ratio of the D and G bands (I_D/I_G) was calculated as 1.04 for NiS_x/C-600, 0.93 for NiS_x/C-700 and 0.85 for NiS_x/C-780, showing that the graphitization degree increases with the calcination temperature [27]. The relatively high graphitization degree may enhance electrocatalytic performance.

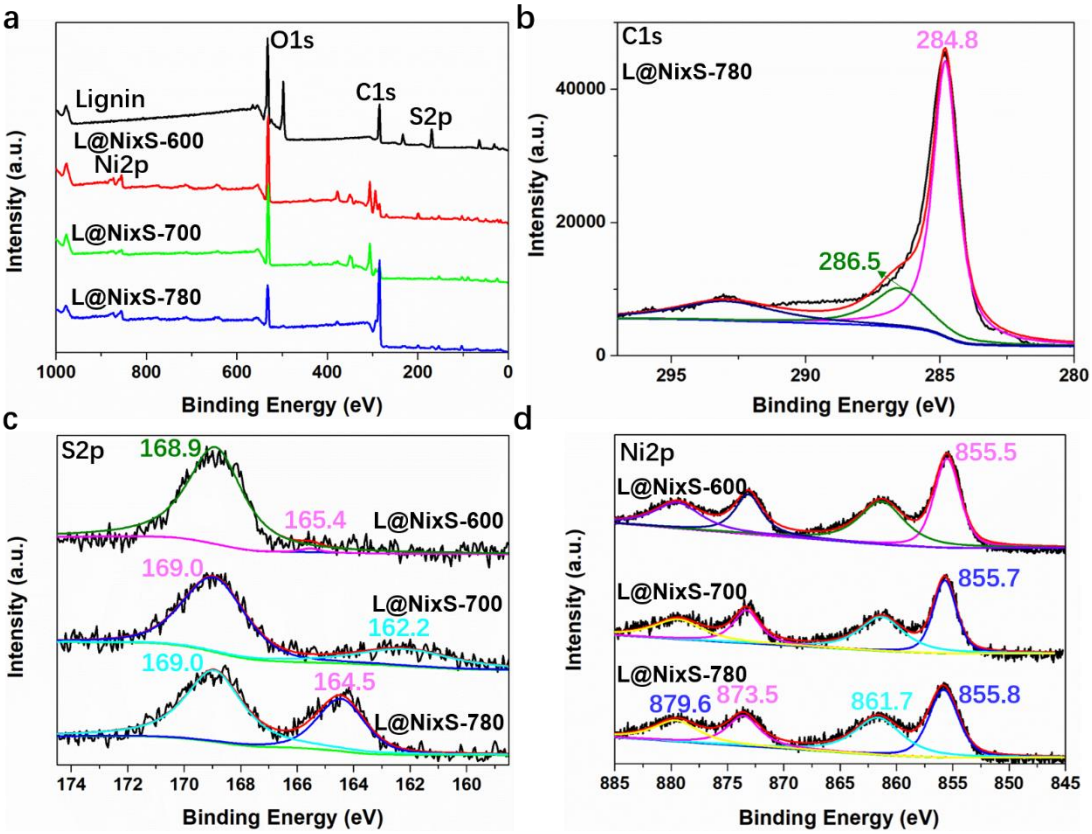

Figure 4. (a) XPS survey spectra of lignin, NiS_x/C-600, NiS_x/C-700 and NiS_x/C-780; (b) C1 s XPS spectrum of CA@Fe(1:3)-800; (c) S2p XPS spectra of NiS_x/C-600, NiS_x/C-700 and NiS_x/C-780; and (d) Ni2p XPS spectra of NiS_x/C-600, NiS_x/C-700 and NiS_x/C-780

Fig. 4a shows the XPS survey curves of lignin, NiS_x/C-600, NiS_x/C-700 and NiS_x/C-780. All the the NiS_x/C-y samples exhibit Ni2p peaks that do not appear in the lignin spectra, confirming the successful growth of Ni_xS on lignin. Fig. 4b shows the C1 s curve of NiS_x/C-780, where the 284.8-eV and 286.5-eV peaks correspond to graphitic carbon and C-O, respectively [28]. We identified differences among the NiS_x/C-y samples by analyzing the corresponding S2p XPS curves, as shown in Fig. 4c. For NiS_x/C-780, the 164.5-eV peak is attributed to C-S-C (S2p3/2 and S2p1/2), and the 169.0-eV peak is ascribed to the oxidized state of S [29]. However, the relative content of C-S-C is quite low for NiS_x/C-600 and NiS_x/C-700, especially for NiS_x/C-600. The presence of S can increase the surface hydrophilicity of carbon materials, thus facilitating charge transfer between the electrolyte and electrode [30]. The high S2p1/2 content for NiS_x/C-600 and NiS_x/C-700 relative to NiS_x/C-780 also suggests a

low Ni_xS content for NiSx/C-780. Fig. 4d shows the Ni2p spectra of NiSx/C-y. The peaks at 855.8 eV and 861.7 eV for NiSx/C-780 are ascribed to Ni2p3/2, whereas the peaks at 873.5 eV and 879.6 eV are attributed to Ni2p1/2 [31]. By comparison with the NiS_x/C-600 spectra, the NiS_x/C-700 and NiS_x/C-780 spectra are shifted to higher binding energies for Ni2p1/2 to different extents, which may enhance electrocatalytic properties.

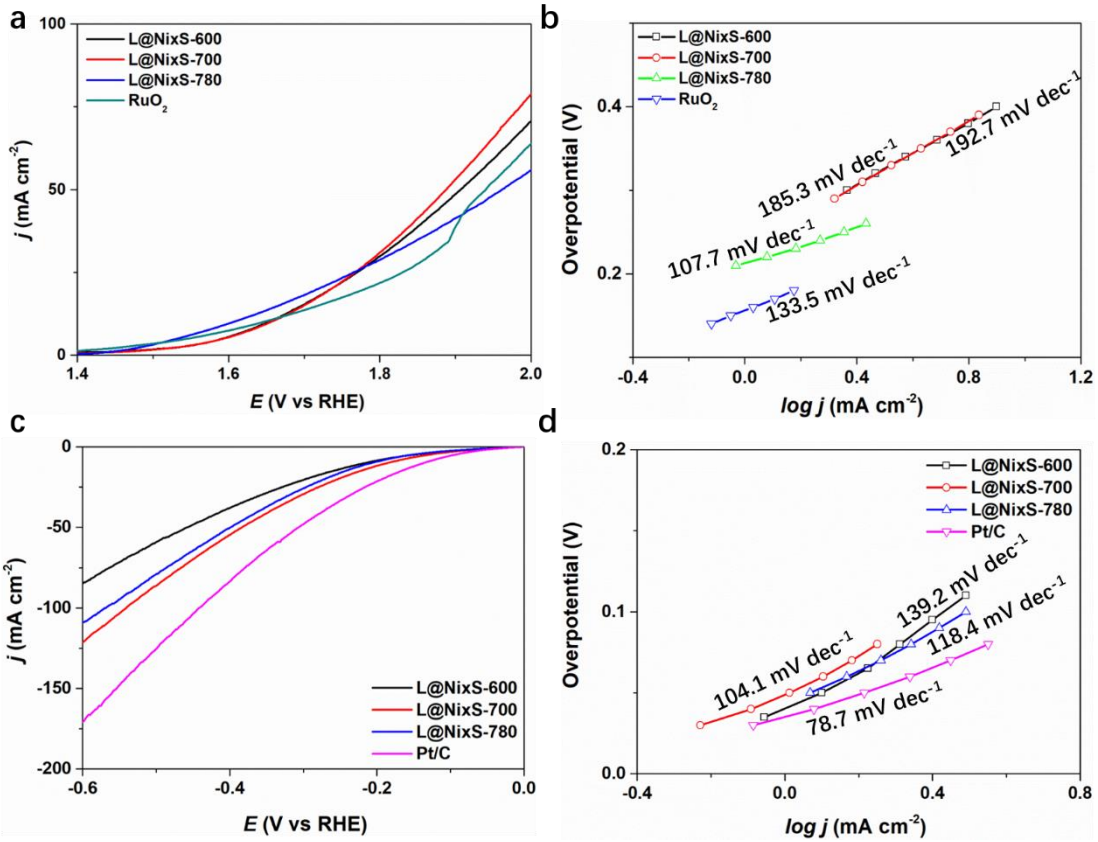

Figure 5. (a) OER LSV curves and (b) Tafel curves of NiS_x/C-600, NiS_x/C-700, NiS_x/C-780 and RuO_2 electrodes; (c) HER LSV curves and (d) Tafel curves of NiS_x/C-600, NiS_x/C-700, NiS_x/C-780 and Pt/C electrodes

Fig. 5 shows the OER and HER performances of all the samples in 1 M KOH. The OER LSV curves presented in Fig. 4a show that the overpotential of NiSx/C-780 is 358 mV at 10 mA cm^{-2}, which is lower than those of RuO_2 (389 mV) and some other electrocatalysts, as shown in Table 1. However, the overpotentials of NiS_x/C-600 and NiS_x/C-700 of 406 mV and 403 mV at 10 mA cm^{-2}, respectively, are slightly higher than that of RuO_2. We also analyzed the Tafel curves of the materials. NiS_x/C-780 exhibits the smallest Tafel slope of 107.7 mV dec^{-1}, which is in accordance with the overpotential data. The Tafel slopes of NiSx/C-600 and NiS_x/C-700 are 192.7 mV dec^{-1} and 185.3 mV dec^{-1}, respectively, showing that NiS_x/C-780 exhibits the best OER performance among all the samples. The HER LSV curves presented in Fig. 5c show that the control group, the Pt/C electrocatalyst, exhibits the lowest overpotential of 118 mV at 10 mA cm^{-2}, which surpasses those of all the NiS_x/C-y materials. Herein, the overpotentials of NiS_x/C-700 and NiS_x/C-780 are 145 mV and 153 mV at 10 mA cm^{-2}, and the

corresponding Tafel slopes for the samples shown in Fig. 5d are slightly different at 104.1 mV dec^{-1} and 118.4 mV dec^{-1}, respectively, and are both larger than that of the Pt/C electrocatalyst (78.7 mV dec^{-1}).

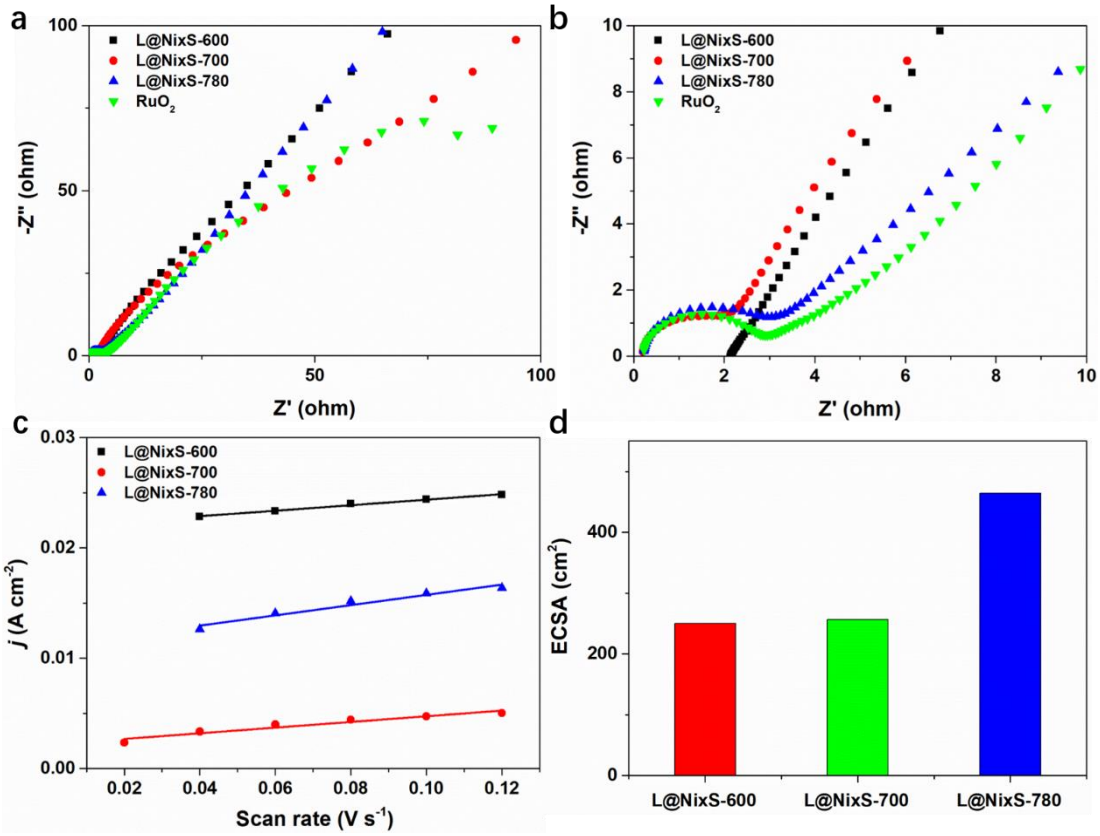

Figure 6. (a) Nyquist plots; (b) Nyquist plots in high-frequency region; (c) current density for different scan rates (0.02~0.12 V s^{-1}); and (d) ECSA of NiS_x/C-600, NiS_x/C-700 and NiS_x/C-780 electrodes

Table 1. Comparison of OER overpotentials of various electrocatalysts in three-electrode system.

Electrocatalyst	Overpotential (mV)	References
$NiCoO_2$-carbon composite	366	32
Mesoporous Co_3O_4 nanowires	405	33
NPCSS	358	34
NiS_x/C-780	358	This work

Figs. 6a and 6b show the measured electrochemical impedance of all the samples. Fig. 6b shows that in the high-frequency region, NiS_x/C-600 is mainly controlled by the solution resistance (R_s),

whereas NiS_x/C-700, NiS_x/C-780 and RuO_2 appear to be controlled by both the transfer resistance (R_{ct}) and the solution resistance. The R_s and R_{ct} of NiS_x/C-700 are 0.20 Ω and 1.87 Ω, respectively, which sum to a total impedance of 2.07 Ω, which is smaller than those of NiS_x/C-780 (3.05 Ω) and RuO_2 (3.01 Ω). Fig. 6c shows a fit to the current density (*j*) data obtained at different scan rates (0.02, 0.04, 0.06, 0.08, 0.10 and 0.12 V s^{-1}). The slope of the fitted curve corresponds to $2C_{dl}$, where C_{dl} is the double layer capacitance; we used double layer capacitance theory to calculate the electrochemically active surface (ECSA). The equation for the ECSA is given below:

$$ECSA = C_{dl}/C_s ,$$

where C_s is 0.04 mF cm^{-2} [35].

The calculated results are shown in Fig. 6d. NiS_x/C-780 has the largest ECSA (464 cm^2), suggesting that NiS_x/C-780 has the largest number of active sites among all the samples [36]. Therefore, NiS_x/C-780 exhibits superior electrocatalytic performance to the NiS_x/C-600 and NiS_x/C-700 samples.

4. CONCLUSIONS

In summary, lignin is used as a carbon source to prepare carbon-based electrocatalysts. The as-obtained NiS_x/C-780 exhibits good OER electrocatalytic properties, with an overpotential of 358 mV at 10 mA cm^{-2} and a Tafel slope of 107.7 mV dec^{-1}, which are superior to those of commercial RuO_2. This study provides a sustainable means of designing carbon-based electrocatalyst materials for water splitting.

ACKNOWLEDGEMENTS
This work was supported by the National Natural Science Foundation of China (No. 21908086 and 51809129), Natural Science Foundation of the Jiangsu Higher Education Insitutions of China (19KJB610011).

CONFLICT OF INTEREST
The authors claim that the researchers in this study have no conflict of interest.

References

1. F. Dawood, M. Anda and G. M. Shafiullah, *Int. J. Hydrogen Energy*, 45 (2020) 3847-3869.
2. S. Y. Tee, K. Y. Win, W. S. Teo, L.-D. Koh, S. Liu, C. P. Teng and M.-Y. Han, *Adv. Sci.*, 4 (2017) 5.
3. X. Sun, X. Liu, R. Liu, X. Sun, A. Li and W. Li, *Catal. Commun.*, 133 (2020) 105826.
4. J. Yin, J. Jin, M. Lu, B. Huang, H. Zhang, Y. Peng, P. Xi and C. H. Yan, *J. Am. Chem. Soc.*, 142 (2020) 18378-18386.
5. Z. Ma, Y. Zhang, S. Liu, W. Xu, L. Wu, Y.-C. Hsieh, P. Liu, Y. Zhu, K. Sasaki, J. N. Renner, K. E. Ayers, R. R. Adzic and J. X. Wang, *J. Electroanal. Chem.*, 819 (2018) 296-305.
6. J. Yu, Q. He, G. Yang, W. Zhou, Z. Shao and M. Ni, *ACS Catal*., 9 (2019) 9973-10011.
7. B. Yan, Z. Chen and Y. Xu, *Chem. - Asian J*., 15 (2020) 2329-2340.
8. C. Tang, M.-M. Titirici and Q. Zhang, *J. Energy Chem*., 26 (2017) 1077-1093.
9. Z. Chen, X. An, L. Dai and Y. Xu, *Nano Energy*, 73 (2020) 104762.

10. X.-l. You, L.-j. Liu, M.-y. Zhang, M. D. Walle, Y. Li and Y.-N. Liu, *Mater. Lett.*, 217 (2018) 167-170.
11. Z. Zhang, S. Yang, H. Li, Y. Zan, X. Li, Y. Zhu, M. Dou and F. Wang, *Adv. Mater.*, (2018) e1805718.
12. X. Ma, C. Ding, D. Li, M. Wu and Y. Yu, *Cellulose*, 25 (2018) 4743-4755.
13. Y.-J. Wang, H. Fan, A. Ignaszak, L. Zhang, S. Shao, D. P. Wilkinson and J. Zhang, *Chem. Eng. J.*, 348 (2018) 416-437.
14. J. Yin, C. Zhang, X. Zhao, H. Yu, Y. Sun and Y. Wang, *Mater. Lett.*, 264 (2020) 127328.
15. H.-G. Jo and H.-J. Ahn, *Catalysts*, 10 (2020) 1316.
16. J. Kim, D. H. Lee, Y. Yang, K. Chen, C. Liu, J. Kang and O. L. Li, *Catalysts*, 10 (2020) 1290.
17. Q. Hu, G. Li, Z. Han, Z. Wang, X. Huang, X. Chai, Q. Zhang, J. Liu and C. He, *Adv. Energy Mater.*, (2019) 1901130.
18. W. Zhao, L.-P. Xiao, G. Song, R.-C. Sun, L. He, S. Singh, B. A. Simmons and G. Cheng, *Green Chem.*, 19 (2017) 3272-3281.
19. O. Yu and K. H. Kim, *Appl. Sci.*, 10 (2020) 4626.
20. J. Xu, C. Li, L. Dai, C. Xu, Y. Zhong, F. Yu and C. Si, *ChemSusChem*, 13 (2020) 4284-4295.
21. L. Xu, S.-J. Zhang, C. Zhong, B.-Z. Li and Y.-J. Yuan, *Ind. Eng. Chem. Res.*, 59 (2020) 16923-16938.
22. J. Rajesh Banu, S. Kavitha, R. Yukesh Kannah, T. Poornima Devi, M. Gunasekaran, S. H. Kim and G. Kumar, *Bioresour. Technol.*, 290 (2019) 121790.
23. X. Q. Wei, Y. L. Wang and G. M. Qu, *Ionics*, 26 (2019) 895-903.
24. H. Wang, M. Liang, D. Duan, W. Shi, Y. Song and Z. Sun, *Chem. Eng. J.*, 350 (2018) 523-533.
25. Q. Hu, X. Zou, Y. Huang, Y. Wei, YaWang, F. Chen, B. Xiang, Q. Wu and W. Li, J. *Colloid Interface Sci.*, 559 (2020) 115-123.
26. L. G. Bulusheva, A. V. Okotrub, I. A. Kinloch, I. P. Asanov, A. G. Kurenya, A. G. Kudashov, X. Chen and H. Song, *Phys. Status Solidi B*, 245 (2008) 1971-1974.
27. Q. Chen, X. F. Tan, Y. G. Liu, S. B. Liu, M. F. Li, Y. L. Gu, P. Zhang, S. J. Ye, Z. Z. Yang and Y. Y. Yang, *J. Mater. Chem. A*, 8 (2020) 5773-5811.
28. H. Peng, B. Yao, X. Wei, T. Liu, T. Kou, P. Xiao, Y. Zhang and Y. Li, *Adv. Energy Mater.*, (2019) 1803665.
29. D. Li, Y. Jia, G. Chang, J. Chen, H. Liu, J. Wang, Y. Hu, Y. Xia, D. Yang and X. Yao, *Chem*, 4 (2018) 2345-2356.
30. L. Hu, J. Hou, Y. Ma, H. Li and T. Zhai, *J. Mater. Chem. A*, 4 (2016) 15006-15014.
31. A. Nairan, P. Zou, C. Liang, J. Liu, D. Wu, P. Liu and C. Yang, *Adv. Funct. Mater.*, 29 (2019) 1903747.
32. C. C. L. McCrory, S. Jung, J. C. Peters and T. F. Jaramillo, *J. Am. Chem. Soc.*, 135 (2013) 16977-16987.
33. Y. Wang, Z. Ge, X. Li, J. Zhao, B. Ma and Y. Chen, *J. Colloid Interface Sci.*, 567 (2020) 308-315.
34. J. Su, G. Xia, R. Li, Y. Yang, J. Chen, R. Shi, P. Jiang and Q. Chen, *J. Mater. Chem. A*, 4 (2016) 9204-9212.
35. Y. Wang, T. Zhou, K. Jiang, P. Da, Z. Peng, J. Tang, B. Kong, W.-B. Cai, Z. Yang and G. Zheng, *Adv. Energy Mater.*, 4 (2014) 16.
36. H. S. Hu, S. Si, R. J. Liu, C. B. Wang and Y. Y. Feng, *Int. J. Energy Res.*, 44 (2020) 9222-9232.